Numerical Study of Plasma Depletion Region in a Satellite Wake

Usui, Hideyuki
Miyake, Yohei
Miloch, J. Wojciech
Ito, Keisuke

Numerical study of plasma depletion region in a satellite wake

Hideyuki Usui, Yohei Miyake, Wojciech J. Miloch and Keisuke Ito

***Abstract*— We demonstrated the existence of a distorted plasma depletion region in a satellite wake through three-dimensional electrostatic particle-in-cell (PIC) plasma simulations. It is commonly known that a wake is formed in the downstream region of a satellite in a magnetized plasma flow. Our simulation shows that the plasma depletion region in the wake is distorted in the plane perpendicular to the static magnetic field. This distortion is asymmetric with respect to the plasma flow direction in the satellite rest frame of reference. We found that the asymmetric structure of the plasma depletion region is caused by non-uniform local drift motion of electrons around the depletion region. By test particle simulations in which electron trajectories are traced in fixed fields obtained in the PIC simulation, we confirmed that cold electrons which have a Larmor radius less than the size of the satellite can cause the asymmetric structure of the plasma depletion in the wake.**

***Index Terms*— satellite wake, particle-in-cell simulation, plasma depletion**

I. INTRODUCTION

IN low-Earth orbit (LEO), the satellite plasma environment is disturbed by the presence of satellites and their relative motion to the background plasma [1]. The disturbance is mainly caused by satellite charging, which is induced by charge accumulation on the satellite surface (e.g. [2][3]). LEO satellite charging and associated plasma disturbances in the vicinity of satellites have been studied by theoretical methods (e.g. [4][5]), numerical simulations (e.g. [6][7]) and rocket and satellite experiments in space (e.g. [8][9]). In the ionosphere, a satellite is negatively charged with respect to the background plasma potential because the electron flux on the satellite surface is much larger than that of ions [10]. Depending on the satellite potential, the ionospheric plasma surrounding the satellite or rocket may be influenced, and a plasma non-uniform region called a sheath is created near the surface to shield the satellite charging (e.g. [7] [11]). The thickness of the plasma sheath is of the order of the plasma Debye length. In the ionosphere, the typical plasma Debye length can be around one cm while the diameter of a rocket or satellite is several tens of cms or more. In this situation, the plasma sheath created around a satellite surface is much thinner than the satellite dimensions. However, when a relative motion exists between a satellite and the background plasma, the region of the plasma disturbance is extended and a plasma perturbation region called a wake is created in the downstream region of the satellite (e.g. [8]). Meanwhile, rockets and satellites spin to stabilize their orientation, and scientific instruments such as Langmuir probes or electric field antennae attached to a satellite surface or booms sticking out of the surface may be affected by the wake region during the satellite spin. Then, the wake interference for these instruments may affect data measurements with regard to plasma density, velocity and fields (e.g. [12][13][14]).

To understand the influence of plasma disturbances, such as wakes, on the data obtained by a satellite, it is important to investigate and understand the wake formation process and its characteristics quantitatively. A promising method for investigating a plasma disturbance in the vicinity of a satellite is a numerical simulation using the particle-in-cell (PIC) method (e.g. [15][16]). In a simulation region filled with background plasma, an internal boundary representing a satellite surface is defined and the charging and associated plasma disturbances such as sheaths and wake formation are simulated in a self-consistent manner. To date, several studies have been performed focusing on wake formation and the characteristics by numerical simulations (e.g. [6][17]). However, the electron dynamics in wake regions have not yet been examined in detail [18]. In this study, we perform three-dimensional electrostatic PIC simulations to examine a wake, considering in particular the plasma depletion region in the wake from the viewpoint of electron dynamics. To investigate the electron motion in detail, we performed a test particle simulation (e.g. [19]) in which the particle trajectories are solved in a region where the field values are fixed at each spatial grid point.

Submission date for review: DD MM YYYY

H. Usui is with Graduate School of System Informatics, Kobe University, 1-1 Rokkodai-cho, Nada-ku, Kobe, Japan (e-mail: h-usui@port.kobe-u.ac.jp).

Y. Miyake is with Education Center on Computational Science and Engineering, Kobe University, 7-1-48 Minatojima minamimachi, Chuo-ku, Kobe, Japan (e-mail: y-miyake@eagle.kobe-u.ac.jp)

W. J. Miloch is with Department of Physics, University of Oslo, P.O. Box 1048 Blindern, 0317 Oslo, Norway (e-mail: w.j.miloch@fys.uio.no)

K. Ito is a graduate student in Graduate School of System Informatics, Kobe University, 1-1 Rokkodai-cho, Nada-ku, Kobe, Japan

TABLE I
Simulation Parameters

	Notations	Values
Mass ratio between ion and electron	m_i/m_e	500
Plasma density	n_0	1.0×10^5 [cm^{-3}]
Electron and ion temperatures	T_e, T_i	3000, 1500 [K]
Ratio between electron thermal velocity and plasma flow velocity	v_{the}/v_{flow}	7.25
Ratio between ion thermal velocity and plasma flow velocity	v_{thi}/v_{flow}	0.23
Mach number	M_0	4.36
Ratio between electron cyclotron frequency and plasma frequency	Ω_e/ω_{pe}	0.49
Ratio between grid size and the Debye length	$\Delta r/\lambda_D$	0.6
Simulation domain	$L_x \times L_y \times L_z$	$(75.5\lambda_D)^3$
Satellite size	$S_x \times S_y \times S_z$	$(11.8\lambda_D)^3$

In section II, we introduce the simulation set up for this study. To simulate satellite charging and the associated plasma disturbance, we immersed a conducting cube representing a satellite in a magnetized plasma flow in the simulation domain. In section III, we present simulation results in terms of density and potential around the satellite to examine the plasma disturbances, such as a wake and plasma depletion. In section IV, we discuss the distortion of the plasma depletion region in the wake shown in section III. In Section V, we summarize this study.

II. SIMULATION SETUP

In the numerical simulations in this study, we used the plasma particle simulation code EMSES (Electro-Magnetic Spacecraft Environment Simulator) [20], which uses the PIC method and solves bunches of charged particles' motions and the electromagnetic fields assigned at spatial grid points by the equations of motion and Maxwell's equations, respectively, by a finite-difference time-domain scheme. Since electrostatic phenomena are important in this study, we solved the Poisson equation for the electrostatic potential defined at each grid point instead of solving the full set of Maxwell's equations. A unique feature of EMSES is that conducting objects can be defined as internal boundaries in the simulation domain filled with plasma. To realize an equipotential surface for the conducting objects, the capacity matrix method [21] is adopted, which qualitatively relates the charges and potential on the satellite surface.

Fig. 1 shows the three-dimensional simulation model used for this study and Table I lists the simulation parameters. We set the spatial grid size Δr to 1 cm, which corresponds to 0.59 λ_D, where λ_D denotes the Debye length of the

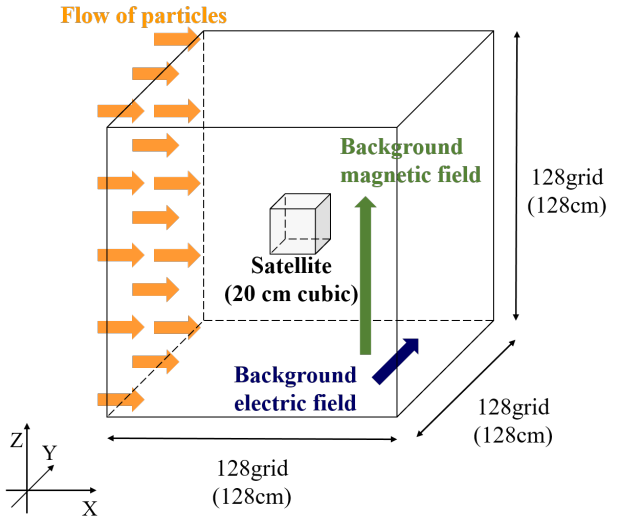

Fig. 1. Three-dimensional simulation model. The plasma flow $\boldsymbol{v}_{flow}$ and uniform magnetic field $\boldsymbol{B_0}$ are in the $+x$ direction and $+z$ direction, respectively. A satellite is located in the center of the simulation domain.

background plasma. The three-dimensional simulation domain therefore is $75.5\lambda_D$ on each side, equivalent to 128 cm. In the center of the simulation region, we set a $11.8\lambda_D$ cubic satellite, corresponding to 20 cm, with a perfectly conducting surface. The amount of plasma passing through the satellite surface is measured and charges are accumulated on the surface. To

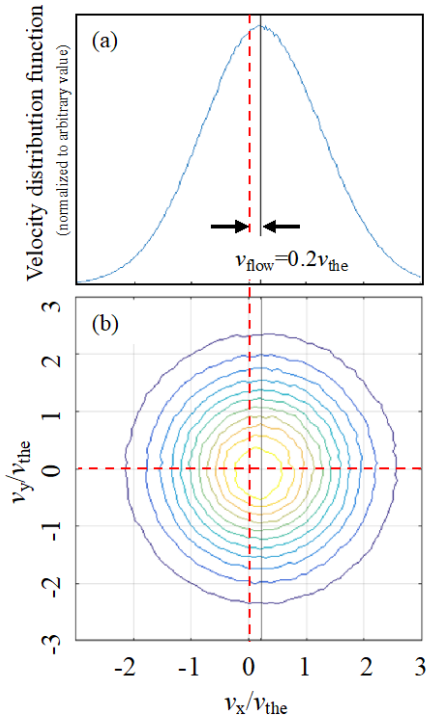

Fig. 2. Electron velocity distribution functions observed at the simulation boundary, where thermal electrons with a drift velocity $\boldsymbol{v}_{flow}$ are injected (x=0) in a test simulation. (a) Drifting Maxwellian distribution function of v_x. (b) Two-dimensional velocity distribution function in the v_x–v_y phase plane, perpendicular to B_0.

realize an equipotential on the satellite surface, the accumulated charges are redistributed on the surface using the capacity matrix method. We focus on direct interactions between the background plasma and the satellite, and no photoelectrons are emitted from the satellite surface and we ignored the effect of photoelectrons on the satellite wake. To simulate a satellite moving through a background plasma, we adopted a satellite rest frame of reference and assigned a relative velocity $\boldsymbol{v}_{flow}$ to the background plasma. In the simulation, instead of real electrons and ions as particles, we introduced a large number of superparticles [20], each of which represents a bunch of real charged particles with the Debye shielding characteristics of plasma. We used 64 superparticles per spatial grid. The background plasma with thermal velocities, shown in Table I, is constantly injected with plasma drift velocity $\boldsymbol{v}_{flow}$ from the left boundary plane in the x direction. To save the computational time, the mass ratio between ions m_i and electrons m_e is set to 500 in the simulation, while oxygen ions (O^+) are dominant in the ionosphere and the realistic mass ratio is 29,376. We set the plasma Mach number M_0, which is the ratio of $\boldsymbol{v}_{flow}$ to the ion acoustic velocity, to be similar to the realistic value of 4.36. Since the wake structure is characterized by M_0, the basic physics for the wake formation are maintained even with the reduced mass ratio plasma.

The static magnetic field $\boldsymbol{B}_0$ representing the geomagnetic field is uniformly set along the z direction. Since we take the satellite rest frame of reference, in which the background plasma exhibits a drift motion perpendicular to $\boldsymbol{B}_0$, a convection electric field $\boldsymbol{E}_0$ should be observed. $\boldsymbol{E}_0$ is perpendicular to $\boldsymbol{B}_0$, satisfying $-\boldsymbol{v}_{flow} \times \boldsymbol{B}_0$, and is set in the simulation domain along the y direction, as shown in Fig. 1.

The background ions and electrons injected from the x=0 plane into the simulation domain follow a drifting Maxwellian velocity distribution along the x direction with a drifting velocity $\boldsymbol{v}_{flow}$ equal to $\boldsymbol{E}_0 \times \boldsymbol{B}_0$. Then, particles taken from the drifting Maxwellian velocity distribution are smoothly injected from the boundary without any unnecessary $\boldsymbol{v} \times \boldsymbol{B}$ field generation.

To examine the electron velocity distribution functions at the boundaries, we performed a test simulation using a simulation model in which a uniform plasma flows with $|\boldsymbol{v}_{flow}| = 0.2v_{\mathrm{the}}$ and no satellite is set in the domain. Fig. 2 shows the electron velocity distribution functions observed in the x=0 plane, which corresponds to the particle injection boundary. As is clearly shown in the figure, a drifting Maxwellian distribution is realized at the boundary, including negative v_x components. At the boundary, electrons with negative v_x components are not injected into the simulation domain. However, to compensate for the negative part of the distribution function, electrons with negative v_x components are introduced from an internal simulation domain where a Maxwellian velocity distribution has already been formed. Panel (b) of Fig. 2 confirms that a drifting Maxwellian velocity distribution is formed in the v_x–v_y phase space at the simulation boundary.

At the downstream outflow boundary, particles exiting through the boundary are removed from the simulation domain. We examined the velocity distribution function, although this is not displayed, and confirmed the same drifting Maxwellian distribution function as observed at the inflow boundary shown in Fig. 2. This is because thermal electrons with negative v_x component are injected from the outflow boundary to the simulation domain. The ratio of the electron cyclotron frequency to the electron plasma frequency, Ω_e/ω_{pe}, in the plasma flow is set to 0.49. We performed the EMSES simulation until a steady state is reached in terms of density variation.

In addition to the EMSES simulation, we performed so-called test particle simulations [19], which enable us to examine the particle trajectories with field components fixed as constant values at grid points. We used the same simulation domain as used in the EMSES simulation and assigned the field data obtained at the final time step in the EMSES simulation. We then placed a charged test particle near the left boundary plane shown in Fig. 1 with an arbitrary initial velocity and continued to solve the equation of motion to trace the particle trajectory.

III. SIMULATION RESULTS

Fig. 3 shows the time variation of the satellite potential obtained in the EMSES simulation. It is seen that the potential quickly drops to −0.6 V as soon as the simulation starts. It then increases slightly and reaches a constant value −0.52 V after 5×10^{-6} s. Considering that the electron thermal velocity is larger than $\boldsymbol{v}_{flow}$, the electron flux entering the satellite is dominant at the beginning of the simulation and the potential quickly drops. Then, the electron flux to the satellite also reduces because of the negative potential, and it eventually becomes the same as the ion flux into the satellite. In other words, the net current at the surface becomes zero at some negative potential that corresponds to the floating potential. We define a steady state after 5×10^{-6} s because the floating

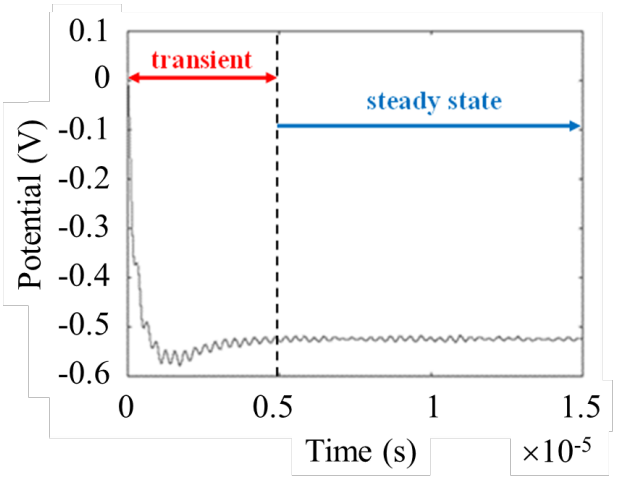

Fig. 3. Time variation of the satellite potential. We define the steady state as the time period when the envelope of the potential variation shows no large changes in the temporal evolution. The steady sate is reached after approximately 5×10^{-6} [s].

potential is obtained for the satellite after that time in the simulation.

Fig. 3 also shows that a small oscillation is overlapped on the potential variation. Although not displayed, we confirmed that the oscillation mainly contains a frequency component of the upper hybrid frequency f_{UHR}. Since the relative motion between the satellite and the background plasma is perpendicular to the static magnetic field $\boldsymbol{B}_0$, the plasma flux at the satellite surface, particularly at the upstream side, determines the satellite potential. In this case, it is no surprise that the potential variation contains an f_{UHR} oscillation [14][22].

Fig. 4 shows contour maps of the electron density, charge density and electric potential in the x–y plane, including the center of the simulation domain. Panel (a), for the electron density, clearly shows a wake structure in the downstream region. The Mach cone angle, calculated from M_0, is $\theta \approx 13.3°$, and the region of the downstream plasma perturbation expands with an angle that almost corresponds to the Mach cone angle. Downstream of the satellite, an electron depletion region is evident, shown in dark blue. It should be noted that the shape of this void in the wake is distorted in the increasing y direction in the panel and shows an asymmetric structure with respect to the plasma flow direction shown by the white dashed line. Although not shown here, the ion density profile also shows a similar asymmetric ion void in the wake region. To clarify the difference between the distributions of electrons and ions, we show the charge density distribution in panel (b) in the same manner as in panel (a). The electron and ion dominant regions are shown in red and blue, respectively. It is clearly seen that the satellite is surround by a blue region except for the downstream side of the satellite. Since the satellite is negatively charged, as shown in Fig. 3, an ion sheath is created around the satellite surface and covers the satellite, shown in blue in panel (b) of Fig. 4. However, negative charges remain downstream of the satellite, which corresponds to the plasma void region. Although it is difficult to see in Fig. 4(a), a small number of electrons are immersed in the void region because they have a larger thermal velocity than the ions. The red region is also asymmetric with respect to the plasma flow direction along the x direction. The potential profile shown in panel (c) also exhibits an asymmetric profile in the downstream region, corresponding to the electron depletion. The panel shows that the potential value at the electron void is more negative than that of the surrounding plasma region.

For a comparison with Fig. 4, we performed another simulation in which no static magnetic field is included. Contour maps of the electron density and electric potential are shown in Fig. 5 in the same manner as in Fig. 4. The profiles for both the electron density and potential in Fig. 5 are almost identical to those in Fig. 4, except for the shape of the electron depletion near the downstream of the satellite. While the electron void is asymmetric with respect to the direction of the plasma flow, as shown in Fig. 4, we can see no asymmetric shape in Fig. 5. This simulation result implies that a static magnetic field can change the shape of the electron depletion

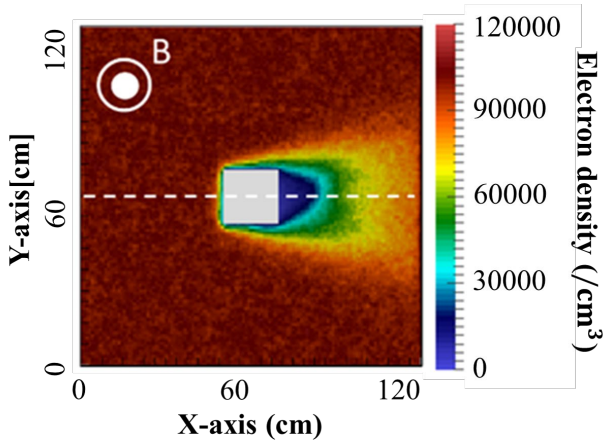

(a) Electron density

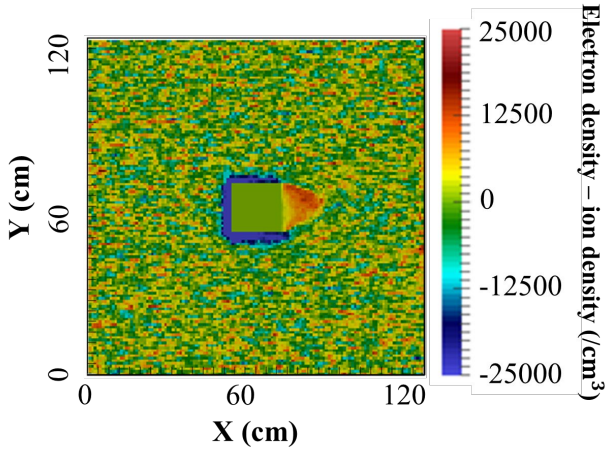

(b) Charge density

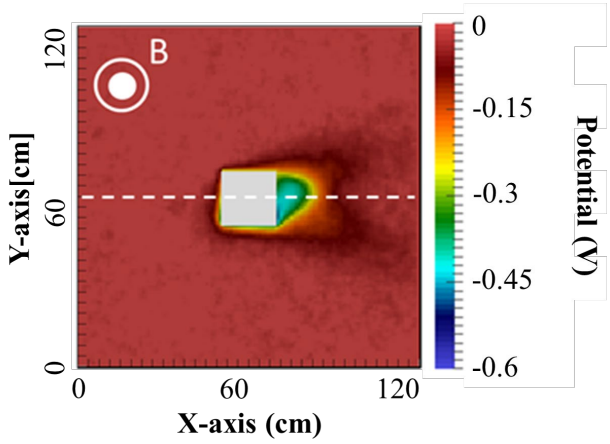

(c) Electric potential

Fig. 4. Contour maps of (a) electron density, (b) charge density and (c) electric potential in the x–y plane, which includes the center of the satellite. The dashed white line indicates the direction of the plasma flow.

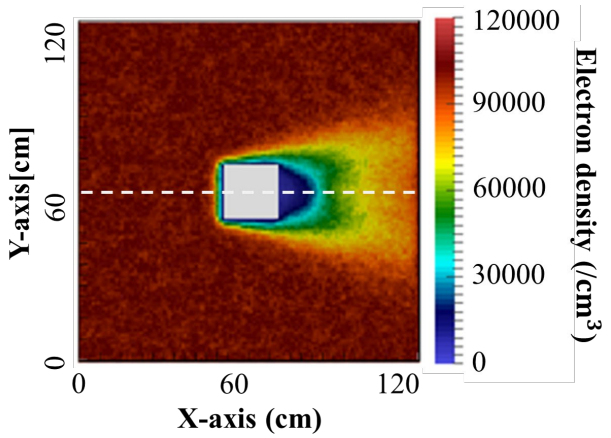

(a) Electron density

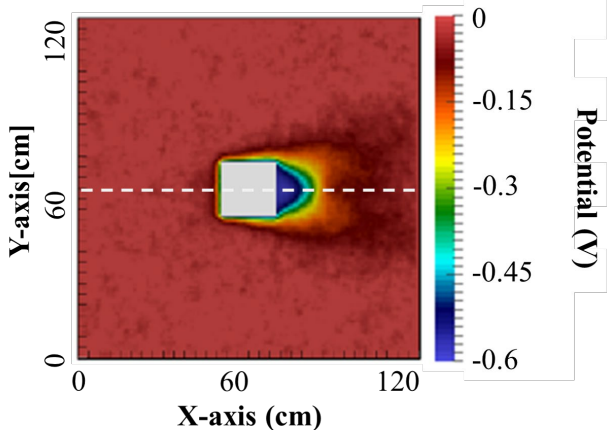

(b) Potential

Fig. 5. Contour maps of (a) electron density and (b) electric potential for the case without a static magnetic field, in the *x*–*y* plane, which includes the center of the satellite. The dashed white line indicates the direction of the plasma flow.

region in the wake. When a static magnetic field $\boldsymbol{B}_0$ is included, an asymmetric electron void is created in the plane perpendicular to $\boldsymbol{B}_0$.

IV. DISCUSSION

We now discuss the asymmetric shape of the electron depletion region in the satellite wake. As shown in Fig. 4, the tail region of the wake near the downstream boundary of the simulation domain is affected by the boundary potential with a fixed value of ϕ=0. To study the tail region of the wake, a larger simulation domain is needed so that the whole wake structure can be covered in the simulation. Regarding the plasma void region near the satellite, however, the distortion of the void is not caused by the boundary effect, but is caused by the effect of $\boldsymbol{B}_0$ on the plasma flow, because no distortion is observed when there is no $\boldsymbol{B}_0$, as shown in Fig. 5.

To examine the void structure and the effect of $\boldsymbol{B}_0$, we analyzed the electron trajectories in the vicinity of the satellite by test particle simulations. As mentioned above, we need the electric and magnetic field values at the final step of the EMSES simulation for the test particle simulations. While the magnetic field is uniform in the simulation, the electric field varies and depends on the region. As shown in Fig. 3, the

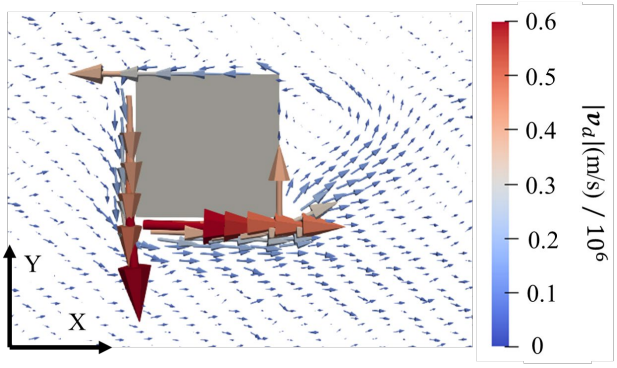

Fig. 6. Vector plot of $\boldsymbol{v}_d = \boldsymbol{v}_{flow} + \boldsymbol{v}_{E\times B}$ in the *x*–*y* plane. The $\boldsymbol{v}_d$ direction is counterclockwise.

satellite potential is negative with respect to the background plasma potential. This implies that the electric field at the satellite surface points inwards into the satellite. In addition, as shown in the contour map of the electric potential in Fig. 4, the electron depletion region has a lower potential than the surrounding region. This indicates that the local electric field at the edge of the plasma depletion region points inwards.

Before the test particle simulations, we examined the average electron flux around the satellite as well as the plasma depletion region in the *x*–*y* plane, which is perpendicular to $\boldsymbol{B}_0$. Since $\boldsymbol{B}_0$ lies along the +*z* direction and the electric field originates at the satellite and the plasma depletion region is in the *x*–*y* plane, the electron $\boldsymbol{E}\times\boldsymbol{B}$ drift motion can be enhanced around the two corresponding regions. To confirm the enhancement of the electron $\boldsymbol{E}\times\boldsymbol{B}$ drift motion, we calculated the $\boldsymbol{E}\times\boldsymbol{B}$ drift velocity $\boldsymbol{v}_{E\times B}$ and plotted it in the *x*–*y* plane, which includes the satellite. Since the background plasma originally has a drift velocity $\boldsymbol{v}_{flow}$, we obtained the total drift velocity $\boldsymbol{v}_d$ as the sum of $\boldsymbol{v}_{flow}$ and the calculated $\boldsymbol{v}_{E\times B}$.

Fig. 6 shows the spatial distribution of the total drift velocity $\boldsymbol{v}_d = \boldsymbol{v}_{flow} + \boldsymbol{v}_{E\times B}$ in the satellite region. The average velocity is indicated as a vector at each grid point. The square in the center represents the satellite. Although it is not clearly shown, $\boldsymbol{v}_d$ is enhanced in the vicinity of the satellite surface, particularly along the surface at the upstream and lower sides of the satellite. The direction of $\boldsymbol{v}_d$ is counterclockwise. Also, $\boldsymbol{v}_d$ circulates around the plasma depletion region. It should be noted that $\boldsymbol{v}_d$ at the lower edge of the void is more intense than at the upper edge. This difference is due to the fact that $\boldsymbol{v}_{E\times B}$ flows in opposite directions in the upper and lower edges of the void in Fig. 6. This difference in $\boldsymbol{v}_d$ means that the structure of the plasma depletion region is distorted and becomes asymmetric with respect to the $\boldsymbol{v}_{flow}$ direction.

We examined this void distortion from the viewpoint of the electron trajectory by test particle simulations. As stated above, we used the electric field profiles obtained for the steady state in the EMSES simulation. To see the dependence of electron trajectories on the initial velocity $\boldsymbol{v}_0 = \boldsymbol{v}_{flow} + \Delta\boldsymbol{v}$, we tested three different $\Delta\boldsymbol{v}$, namely $\boldsymbol{v}_{th}$, $0.5\boldsymbol{v}_{th}$ and $2\boldsymbol{v}_{th}$, where $\boldsymbol{v}_{th}$ represents the electron thermal velocity. The electron

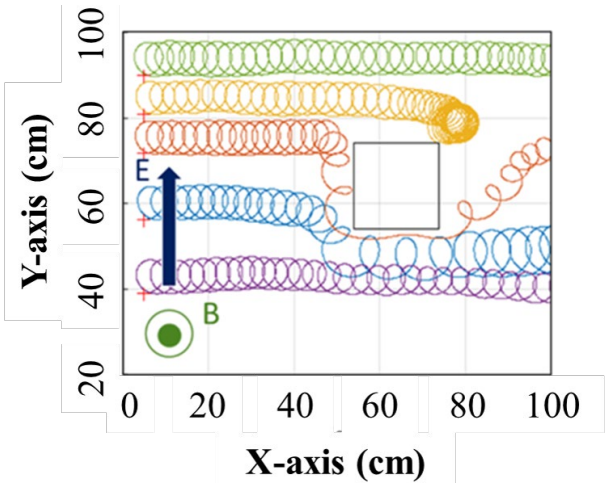

(a) $\Delta \boldsymbol{v} = \boldsymbol{v}_{th}$

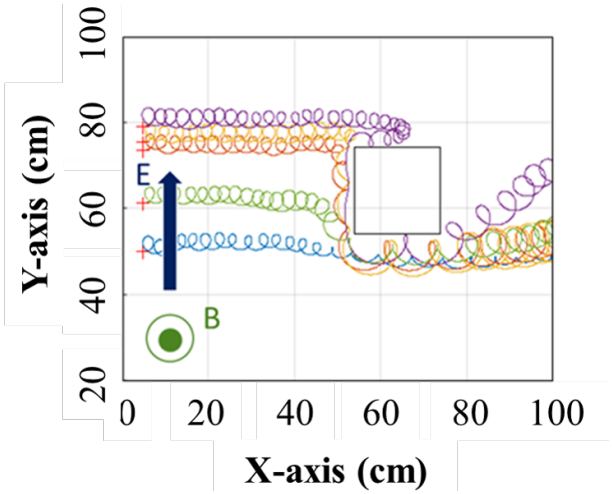

(b) $\Delta \boldsymbol{v} = 0.5\boldsymbol{v}_{th}$

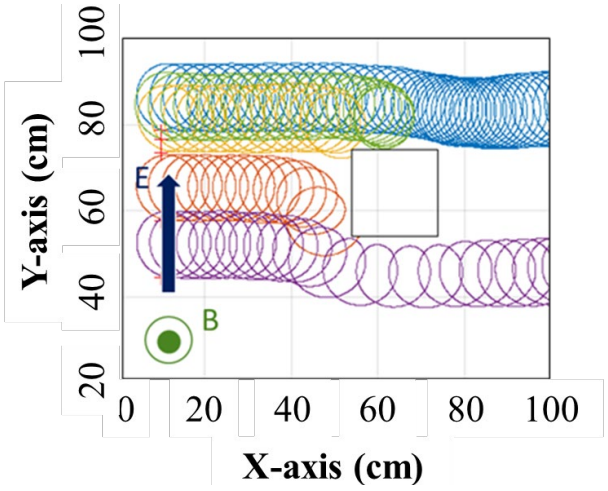

(c) $\Delta \boldsymbol{v} = 2\boldsymbol{v}_{th}$

Fig. 7. Electron trajectories near the satellite with an initial velocity of $\boldsymbol{v}_0 = \boldsymbol{v}_{flow} + \Delta \boldsymbol{v}$ in which (a) $\Delta \boldsymbol{v} = \boldsymbol{v}_{th}$, (b) $\Delta \boldsymbol{v} = 0.5\boldsymbol{v}_{th}$ and (c) $\Delta \boldsymbol{v} = 2\boldsymbol{v}_{th}$. In each case, electrons are initially placed at several different positions in the upstream region.

trajectories for these three cases are shown in panels (a), (b) and (c) of Fig. 7 respectively.

The electron trajectories for the cases $\Delta \boldsymbol{v} = \boldsymbol{v}_{th}$ and $\Delta \boldsymbol{v} = 0.5\boldsymbol{v}_{th}$ are shown in panels (a) and (b), respectively. As shown by the third trajectory from the top for the case of $\Delta \boldsymbol{v} = \boldsymbol{v}_{th}$, electrons approaching the satellite surface stagnate near the surface at the upstream side and move around the satellite in a counterclockwise direction. Downstream, they move in an oblique direction at the lower side of the plasma depletion region. This behavior agrees with the results shown in the vector plot of the drift velocity in Fig. 6. However, the second trajectory from the top shows a different electron passing through the upper side of the satellite and almost stagnating. This means that $\boldsymbol{v}_{flow}$ is canceled by $\boldsymbol{v}_{E\times B}$. We can see similar features in the electron trajectories in the middle panel corresponding to the case $\Delta \boldsymbol{v} = 0.5\boldsymbol{v}_{th}$. In the case of $\Delta \boldsymbol{v} = 2\boldsymbol{v}_{th}$, shown in Panel (c) of Fig. 7, this tendency of the electron motion is not seen because the Larmor radius of the electrons increases and becomes almost the same size as the satellite dimensions, almost comparable to the size of the plasma depletion. However, considering that the population of electrons with velocity larger than $2\boldsymbol{v}_{th}$ is small in the Maxwellian velocity distribution, the number of electron trajectories shown in the bottom panel is small and the electrons shown in panels (a) and (b) are dominant.

When the $\boldsymbol{B}_0$ intensity becomes small and the resulting electron Larmor radius becomes much larger than the satellite size, it is predicted that the distortion of the plasma void region becomes will be hard to observe. As shown in panel (c) of Fig. 7, electrons with Larmor radius comparable to the satellite size easily collide with the satellite surface when they approach the satellite. Electrons moving through at the upper and lower sides of the satellite to the downstream side are less affected by the satellite potential. This implies that the distortion of the electron void region is not caused by the electrons with Larmor radius comparable or larger than the satellite size.

As discussed above, the drift motion around the plasma depletion region is an important factor for accounting for the distortion of the void structure. In the total drift velocity $\boldsymbol{v}_d = \boldsymbol{v}_{flow} + \boldsymbol{v}_{E\times B}$ at the depletion edge, the direction of $\boldsymbol{v}_{E\times B}$ is the same as that of $\boldsymbol{v}_{flow}$ at the lower edge, while it is opposite at the upper edge. Considering that $\boldsymbol{v}_{flow}$ is uniform in the simulation domain, $\boldsymbol{v}_d$ becomes non-uniform around the void such that it becomes stronger at the lower edge of the depletion region while it becomes weak at the upper edge. In this situation, the plasma depletion region is eventually distorted toward the upper side.

The wake structure formed behind the satellite is determined by the Mach number of the plasma flow M_c. When M_c is constant, if we change $\boldsymbol{v}_{flow}$, the structure of the plasma depletion region in the wake changes because the total drift velocity $\boldsymbol{v}_d$ around the void region changes. For example, when we decrease $\boldsymbol{v}_{flow}$ keeping M_c the same, the satellite charging becomes more negative because there is less ion flux coming into the satellite surface. In this situation, the depletion region shrinks because of the slower $\boldsymbol{v}_{flow}$. On the other hand, the electric field at the satellite surface is intensified because

the satellite potential becomes more negative. Then, in the total drift velocity $\boldsymbol{v}_d = \boldsymbol{v}_{flow} + \boldsymbol{v}_{E\times B}$, the contribution of $\boldsymbol{v}_{flow}$ becomes minor and $\boldsymbol{v}_{E\times B}$ around the depletion region becomes dominant. As stated above, however, the depletion region shrinks and it can be difficult to observe.

On the other hand, when we increase $\boldsymbol{v}_{flow}$ keeping M_c the same, the satellite charging decreases because the ion flux to the satellite increases to compensate the electron flux. At the same time, the plasma depletion region in the wake is enlarged because of the large $\boldsymbol{v}_{flow}$. However, since the satellite charging is reduced, the electric field at the satellite becomes weak and eventually $\boldsymbol{v}_{E\times B}$ decreases. Then, in the total drift velocity $\boldsymbol{v}_d$, $\boldsymbol{v}_{flow}$ becomes dominant in comparison with $\boldsymbol{v}_{E\times B}$. Since $\boldsymbol{v}_d$ becomes almost uniform in the wake region, no distortion of the plasma depletion can be found when $\boldsymbol{v}_{flow}$ is large.

Considering the above discussion, there must be some plasma condition in which the distortion of the plasma depletion region is enhanced. To clarify this condition, we need to perform further simulations changing $\boldsymbol{v}_{flow}$ keeping M_c the same, which is left as future work.

Finally, to study the details of the electron dynamics at the edge of the electron depletion region, we examined the electron velocity distribution function. It turned out, however, that the shape of the distribution function is the same as that shown in Fig. 2, observed in the unperturbed region. As indicated by the arrows in Fig. 6, the electron flux at the upper edge of the depletion region is reversed to the negative x direction. The peak of the velocity distribution function can be shifted to the negative $\boldsymbol{v}_x$ domain. However, no shift of the peak is found. A possible reason for this is that the component of the electron reversal flow at the upper edge of the void can only be found on the plane perpendicular to $\boldsymbol{B}_0$, and it may be small and hard to recognize in the electron velocity distribution function in which the components along $\boldsymbol{B}_0$ in the z direction are dominant. If the satellite is not a cube but has a long structure along $\boldsymbol{B}_0$ in the z direction, the electron depletion region can be elongated along the $\boldsymbol{B}_0$ direction and it may be possible to observe the shift of the peak of the electron velocity distribution function to the negative $\boldsymbol{v}_x$ domain at the upper edge of the electron depletion region.

V. SUMMARY

We studied the distortion of the plasma depletion region in the wake of a satellite immersed in a magnetized plasma flow using three-dimensional PIC simulations. In the simulation, we confirmed that the satellite potential becomes negative due to an electron flux into the satellite, and a wake is formed in the downstream region of the satellite. In the wake region, we observed a distorted structure of a plasma depleted region in the plane perpendicular to the static magnetic field $\boldsymbol{B}_0$.

The electric field at the satellite surface and the edge of the depletion region point inward because the potentials of both regions are negative. In the plane perpendicular to $\boldsymbol{B}_0$, the total drift velocity of plasma particles is expressed as $\boldsymbol{v}_d = \boldsymbol{v}_{flow} + \boldsymbol{v}_{E\times B}$, in which $\boldsymbol{v}_{E\times B}$ circulates around the satellite and the plasma void region in the wake. Because the direction of $\boldsymbol{v}_{E\times B}$ differs at each point on the satellite surface as well as the void edge, $\boldsymbol{v}_d$ is non-uniform. In the case in the previous section, $\boldsymbol{v}_d$ becomes larger at the lower side of the plasma depletion region than at the upper side. Because of the non-uniform $\boldsymbol{v}_d$, the plasma depletion region is distorted. Through test particle simulations, we examined the dependence of the initial electron velocity $\boldsymbol{v}_0 = \boldsymbol{v}_{flow} + \Delta\boldsymbol{v}$ on the trajectory in the plane perpendicular to $\boldsymbol{B}_0$. We could confirm that electrons approaching the satellite surface go around the satellite for $\Delta\boldsymbol{v} = \boldsymbol{v}_{th}$ and $\Delta\boldsymbol{v} = 0.5\boldsymbol{v}_{th}$. The electron trajectories for these two cases basically agree with the spatial profile of $\boldsymbol{v}_d$. In the case of $\Delta\boldsymbol{v} = 2\boldsymbol{v}_{th}$, however, we could not observe electron circulation around the satellite because the Larmor radius of the electrons increases to the size of the satellite and the plasma depletion region. We conclude that cold electrons with a Larmor radius less than the size of the satellite can cause a distortion of the plasma depletion in the wake.

VI. REFERENCES

[1] D. Hastings and H. Garrett, *Spacecraft-environment interactions*, United Kingdom: Cambridge University Press, 1996.

[2] P. C. Anderson, "Characteristics of spacecraft charging in low Earth orbit," *JOURNAL OF GEOPHYSICAL RESEARCH-SPACE PHYSICS*, vol. 117, Jul. 2012, DOI: 10.1029/2011JA016875.

[3] C. P. Escoubet, A. Pedersen, and R. Schmidt, "Density in the magnetosphere inferred from ISEE 1 spacecraft potential," *JOURNAL OF GEOPHYSICAL RESEARCH-SPACE PHYSICS*, vol. 102, no. A8, pp. 17595-17609, Aug. 1997, DOI: 10.1029/97JA00290.

[4] H. B. Garrett, "The Charging of Spacecraft Surfaces," *REVIEWS OF GEOPHYSICS*, vol. 19, no. 4, pp. 577-616, 1981, DOI: 10.1029/RG019i004p00577.

[5] M. U. Siddiqui, L. E. Gayetsky, M. R. Mella, K. A. Lynch and M. R. Lessard, "A laboratory experiment to examine the effect of auroral beams on spacecraft charging in the ionosphere," *PHYSICS OF PLASMAS*, vol. 18, no. 9, Sep. 2011, DOI: 10.1063/1.3640512.

[6] D. Darian, S. Marholm, J. J. P. Paulsson, Y. Miyake, H. Usui, M. Mortensen and W. J. Miloch, "Numerical simulations of a sounding rocket in ionospheric plasma: Effects of magnetic field on the wake formation and rocket potential," *JOURNAL OF GEOPHYSICAL RESEARCH-SPACE PHYSICS*, vol. 122, no. 9, pp. 9603-9621, Sep. 2017, DOI: 10.1002/2017JA024284.

[7] C. J. Capon, M. Brown, C. White, T. Scanlon, R.R. Boyce, "pdFOAM: A PIC-DSMC code for near-Earth plasma-body interactions," *COMPUTERS & FLUIDS*, vol. 149, pp. 160-171, Jun. 2017, DOI: 10.1016/j.compfluid.2017.03.020.

[8] M. S. Gussenhoven, D. A. Hardy, F. Rich, W. J. Burke and H. C. Yeh, "HIGH-LEVEL SPACECRAFT CHARGING IN THE LOW-ALTITUDE POLAR AURORAL ENVIRONMENT, " *JOURNAL OF GEOPHYSICAL RESEARCH-SPACE PHYSICS*, vol. 90, no. NA11, pp. 1009-1023, 1985, DOI: 10.1029/JA090iA11p11009.

[9] R. J. Redmon, J. V. Rodriguez, C. Gliniak, and W. F. Denig, "Internal Charge Estimates for Satellites in Low Earth Orbit and Space Environment Attribution," *IEEE TRANSACTIONS ON PLASMA SCIENCE*, vol. 45, no. 8, pp. 1985-1997, Aug. 2017, DOI: 10.1109/TPS.2017.2656465

[10] D. E. Hastings, "A review of plasma interactions with spacecraft in low Earth orbit," *JOURNAL OF GEOPHYSICAL RESEARCH-SPACE PHYSICS*, vol. 100, no. A8, pp. 14457-14483, Aug. 1995, DOI: 10.1029/94JA03358.

[11] V. C. Liu, "Ionospheric gas dynamics of satellites and diagnostic probes," *SPACE SCIENCE REVIEWS*, vol. 9, no. 4, pp. 423-490, 1969, DOI: 10.1007/BF00212707.

[12] A. Spicher, A. A. Ilyasov, W. J. Miloch, A. A. Chernyshov, L. B. N. Clausen, J. I. Moen, T. Abe, and Y. Saito, "Reverse flow events and small-scale effects in the cusp ionosphere," *JOURNAL OF GEOPHYSICAL RESEARCH-SPACE PHYSICS*, vol. 121, no. 10, pp. 10466-10480, Oct. 2016, DOI: 10.1002/2016JA022999.

[13] J. E. Sorensen, N.H. Stone and K. H. Wright Jr., "Change in ion distribution function while crossing the space shuttle wake," *JOURNAL OF GEOPHYSICAL RESEARCH-SPACE PHYSICS*, vol. 102, no. A11, pp. 24117-24126, Nov. 1997, DOI: 10.1029/97JA01869.

[14] K. Endo, A. Kumamoto and Y. Katoh, "Observation of wake-induced plasma waves around an ionospheric sounding rocket," JOURNAL OF GEOPHYSICAL RESEARCH-SPACE PHYSICS, vol. 120, no. 6, pp. 5160-5175, Jun. 2015, DOI: 10.1002/2014JA020047.

[15] C. K. Birdsall and A. B. Langdon, *Plasma Physics via Computer Simulation*, NY, USA: MacGraw-Hill, 1985.

[16] R. W. Hockney and J. W. Eastwood, *Computer Simulation Using Particles*, NY, USA: MacGraw-Hill, 1981.

[17] R. M. Albarran and A. Barjatya, "Plasma Density Analysis of CubeSat Wakes in the Earth's Ionosphere," *JOURNAL OF SPACECRAFT AND ROCKETS*, vol. 53, no. 3, pp. 393-400, May. 2016, DOI: 10.2514/1.A33402.

[18] J. Wang and Y. Hu, "The Breakdown of the Fluid Approximation for Electrons in a Plasma Wake", *JOURNAL OF GEOPHYSICAL RESEARCH-SPACE PHYSICS*, Sep.2018, DOI:10.1029/2018JA025743

[19] R. Marchand, "Test-Particle Simulation of Space Plasmas," *COMMUNICATIONS IN COMPUTATIONAL PHYSICS*, vol. 8, no. 3, pp. 471-483, Sep. 2010, DOI: 10.4208/cicp.201009.280110a.

[20] Y. Miyake and H. Usui, "New electromagnetic particle simulation code for the analysis of spacecraft-plasma interactions," *PHYSICS OF PLASMAS*, vol. 16, no. 6, Jun. 2009, DOI: 10.1063/1.3147922.

[21] M. Melzani, R. Walder, D. Folini and C. Winisdoerffer, "DIFFERENCES BETWEEN REAL AND PARTICLE-IN-CELL PLASMAS: EFFECTS OF COARSE-GRAINING," *International Journal of Modern Physics*, vol. 28, Mar. 2014, DOI: 10.1142/S201019451460194X.

[22] C. A. Colpitts and J. LaBelle, "Mode identification of whistler mode, Z-mode, and Langmuir/Upper Hybrid mode waves observed in an auroral sounding rocket experiment," *JOURNAL OF GEOPHYSICAL RESEARCH-SPACE PHYSICS*, vol. 113, no. A4, Apr. 2008, DOI: 10.1029/2007JA012325.

VII. BIOGRAPHIES

Hideyuki Usui received the Ph.D degree from Department of Electronics, Kyoto University, Japan in 1994. He is currently a professor at the department of the computational science in the graduate school of system informatics, Kobe University, Japan. His research interests include plasma particle simulations of space environment such as spacecraft-plasma interaction, planetary magnetosphere and associated electron dynamics.

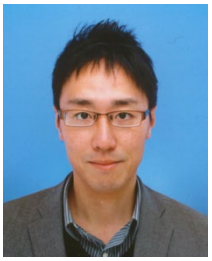

Yohei Miyake received the Ph.D. degree in electrical engineering from the Kyoto University, Japan, in 2009. He is currently an Associate Professor at the Education Center on Computational Science and Engineering, Kobe University. His research interests include space plasmas, plasma interactions with solid objects, and their numerical modeling.

Wojciech J. Miloch received the M.Sc. degree in space and plasma physics and the Ph.D. degree from the University of Oslo, Norway, in 2006 and 2009, respectively. He is currently a professor and head of 4DSpace Strategic Research Initiative at the Department of Physics, University of Oslo. His research interests include space and astrophysical plasmas, space weather, plasma interactions with finite sized objects, such as spacecrafts, probes, or dust grains, complex plasmas and numerical modeling.

Keisuke Ito is currently a graduate student of the master course in the graduate school of system informatics, Kobe University, Japan. He has been working on the analysis of velocity distribution function in space plasma.